Surface Characterization of the Spinel $Li_xMn_2O_4$ Cathode before and after Storage at Elevated Temperatures

Forest T. Quinlan,[†] Keiichiro Sano,[†,‡] Trevor Willey,[§] Ruxandra Vidu,[†] Ken Tasaki,[‡] and Pieter Stroeve*[,†]

Department of Chemical Engineering and Materials Science, University of California, Davis, Davis, California 95616, Department of Physics, University of California, Davis, Davis, California 95616, and MC Research and Innovation Center, Inc., Mountain View, California 940041

Received April 17, 2001. Revised Manuscript Received July 27, 2001

Surface chemistry of the capacity fading of the $Li_xMn_2O_4$ cathode was investigated using atomic force microscopy (AFM), energy-dispersive X-ray analysis (EDAX), and X-ray photoelectron spectroscopy (XPS). Measurements show a decrease in the cathode capacity from 124 mA h g^{-1} *before storage* to 102 mA h g^{-1} *after storage* in an electrolyte of 1 M $LiPF_6$/EC + DMC + DEC at 70 °C for 5 days. Surface morphological changes of the $Li_xMn_2O_4$ cathode were monitored using contact and tapping AFM and lateral force microscopy in air. Nanoscale changes of the charged cathode *before* and *after storage* at 70 °C were observed. *Before storage*, homogeneous grains of approximately 100−200 nm are seen. *After storage*, fine and nearly round shaped structures of 10−30 nm in size are observed covering the larger grains on the surface of the cathode. This change in morphology suggests film deposition on the cathode's surface, which increases the resistance for Li^+ ion transport in and out of the cathode. Results from EDAX show that compounds containing phosphorus and fluorine are also deposited on the surface of the cathode. Surface analysis of the cathode with XPS suggests the presence of MnF_2. The conversion of the oxidation state of manganese on the surface of the cathode from MnO_2 to MnO during storage at the elevated temperature was observed with XPS.

Introduction

The spinel $Li_xMn_2O_4$ is a promising cathode material for rechargeable lithium ion batteries because of its high voltage, low cost, and safety.[1,2] However the $Li_xMn_2O_4$ cathode has problems with capacity fading with cycling at elevated temperatures and especially after storage at elevated temperatures. These problems should be solved before commercial usage. Many studies have been conducted to clarify the mechanism of lithium battery deterioration.[3−5] Capacity fading is thought to be caused by an increase in the cathode resistance. These phenomena may occur through a combination of effects in capacity fading during cycling at elevated temperatures, which include the following: (1) electrolyte decomposition at a voltage range higher than 4 V; (2) dissolution of $Li_xMn_2O_4$ into the electrolyte through the disproportionation reaction of $2Mn^{3+} \rightarrow Mn^{2+} + Mn^{4+}$; (3) irreversible structure transition due to Jahn−Teller distortion at the discharged state; (4) transformation of an unstable two-phase structure in the high-voltage region to a more stable single-phase structure through loss of MnO.[6,7]

Jang et al.[8] reported that Mn dissolution in the cathodes causes capacity fading by two different pathways. The first pathway is a material loss of the loaded spinel, and the second pathway is a polarization loss due to cell resistance increase. Specifically, the resistance increase is due to a high contact resistance at the spinel/carbon interface caused by Mn dissolution. The main cause of the contact resistance is the formation of a film on the surface of the cathode, which reduces Li^+ ions from transferring in and out of the cathode. Investigations on the surface of anodes including intercalation/deintercalation of Li^+ ions have been widely conducted,[9−11] but only a limited number of studies have been conducted on the cathode surface. Blyr et al.[12] obtained scanning electron microscope (SEM) micrographs of $Li_xMn_2O_4$ cathodes left at 55 °C for 2 months and observed a pitted surface due to Mn dissolution.

* To whom correspondence should be addressed. E-mail: pstroeve@ucdavis.edu. Fax: +1-530-752-8778. Phone: +1-530-752-8778.
[†] Department of Chemical Engineering and Materials Science, University of California, Davis.
[‡] MC Research and Innovation Center, Inc.
[§] Department of Physics, University of California, Davis.

(1) Tarascon, J. M.; Guyomard, D. *Electrochim. Acta* **1993**, *38*, 1221.
(2) Tarascon, J. M.; McKinnon, W. R.; Coowar, F.; Bowmer, T. N.; Amatucci, G.; Guyomard, D. *J. Electrochem. Soc.* **1994**, *141*, 1421.
(3) Wen, S. J.; Richardson, T. J.; Ma, L.; Striebel, K. A.; Ross, P. N., Jr.; Cairns, E. J. *J. Electrochem. Soc.* **1996**, *143*, L136.
(4) Xia, Y.; Zhou, Y.; Yoshio, M. *J. Electrochem. Soc.* **1997**, *144*, 2593.
(5) Inoue, T.; Sano, M. *J. Electrochem. Soc.* **1998**, *145*, 3704.
(6) Gummow, R. J.; de Kock, A.; Thackeray, M. M. *Solid State Ionics* **1994**, *69*, 59.
(7) Arora, P.; White, R. E.; Doyle, M. *J. Electrochem. Soc.* **1998**, *145*, 3647.
(8) Jang, D. H.; Shin, Y. J.; Oh, S. M. *J. Electrochem. Soc.* **1996**, *143*, 2204.
(9) Aurbach, D.; Cohen, Y. *Electrochem. Solid-State Lett.* **1999**, *2*, 16.
(10) Aurbach, D.; Weissman, I.; Yamin, H.; Elster, E. *J. Electrochem. Soc.* **1998**, *145*, 1421.
(11) Hirasawa, K. A.; Sato, T.; Asahina, H.; Yamaguchi, S.; Mori, S. *J. Electrochem. Soc.* **1997**, *144*, L81.
(12) Blyr, A.; Sigala, C.; Amatucci, G.; Guyomard, D.; Chabre, Y.; Tarascon, J. M. *J. Electrochem. Soc.* **1998**, *145*, 194.

10.1021/cm010335v CCC: $20.00 © 2001 American Chemical Society
Published on Web 10/12/2001

Antonini et al.[13] studied with SEM a Ga-doped spinel cathode surface *after storage* at 55 °C and concluded that a surface layer is formed during storage with an open circuit following the first charge.

It is imperative to identify the change on the cathode surface to determine the mechanism of capacity fading. In this work, we studied the surface of the spinel cathode with atomic force microscopy (AFM) and investigated the relationship between the micromorphological changes and the electrochemical characteristics. The atomic force microscopy is an effective tool for surface analysis of the actual composite electrode at the micro- and nanoscale level as it provides imaging the surface in various modes. There are several imaging modes that can be used for imaging cathode material surface such as contact AFM for topographic imaging, tapping mode AFM (TM-AFM) that operates by vibrating the cantilever near its resonance frequency, and lateral force (LFM) that images the frictional differences in a sample by detecting the lateral bending of the cantilever as a result of frictional properties. All these imaging techniques are widely recognized and documented. We used these imaging techniques to provide a basis for composite electrode imaging that is important in determining the imaging mode that maximizes the information on surface topography and binder distribution.

Along with the surface topography, we studied the surface chemistry of the cathode. In particular it is useful to investigate what compounds are involved in the formation of the passivating layer as seen by other investigators. To this end, energy-dispersive X-ray analysis (EDAX) and X-ray photoelectron spectroscopy (XPS) were employed to identify the nature of these compounds.

Experimental Section

The cathode material was prepared by mixing 75 wt % of $LiMn_2O_4$ (synthesized by Mitsubishi Chemical Corp.), 20 wt % of acetylene black (Denki Kagaku Kogyo Co. Ltd.), and 5 wt % of Teflon (Mitsui Dupont Fluoro Chemical Co. Ltd.) and was kneaded to a flat sheet with a mortar and a pestle. A cathode pellet was punched out from the sheet into a disk 8 mm in diameter and pressed on an aluminum metal mesh, which was used as the working electrode in the electrochemical measurements. Before assembly of the electrochemical cell, the working electrode was dried at 120 °C in a vacuum oven for 2 h to remove excess water and water vapor, which could react with the electrolyte.

For electrochemical studies, a beaker-type three-electrode cell was used inside an argon atmosphere glovebox. The working electrode was placed in the cell with two pieces of pure Li metal (Alfa Aesar), which was used as the counter and the reference electrodes. The electrolyte used for electrochemical measurements contained 1 mol of $LiPF_6$ in a mixed solvent of ethylene carbonate (EC), dimethyl carbonate (DMC), and diethyl carbonate (DEC). The proportions for EC:DMC:DEC were 2:2:1 by volume (Mitsubishi Chemical Corp.).

Charge/discharge properties of the electrochemical cell were measured with a model HJ-201B charge/discharge unit (Hokuto Denko Corp.) in the voltage range of 3.2 and 4.3 V. Cyclic voltammetry was carried out with a model AFCBP1 bipotentiostat (Pine Co.) between 3.2 and 4.4 V at the sweep rate of 10 mV/min. After the cell was charged, the cathode and a Li metal separated by a polyethylene sheet were placed in a Teflon bottle and immersed in fresh electrolyte and stored in an oven at 70 °C for 2 weeks. The cathode was then extensively rinsed with pure DMC. *Before* and *after storage*, the electrochemical properties of the cell were determined. *After storage*, new Li metal was used to assemble the battery. All sample preparations and measurements were conducted at room temperature (25 °C). The surfaces of the cathode were observed by atomic force microscopy (AFM, Nano Scope IIIA, Digital Instruments) using various imaging modes in air. Before measurements the cathode was extensively rinsed with pure DMC and dried by argon flow in the argon glovebox. For contact AFM and lateral force (LFM), commercially available triangular gold-coated cantilevers with pyramidal tips of 0.05 N/m force constant were used. Rectangular gold-coated Si cantilevers (200 mm length and 0.02 N/m force constant) were used for tapping mode. To correct for tilt and bow, images were processed using the imaging software of the instrument.

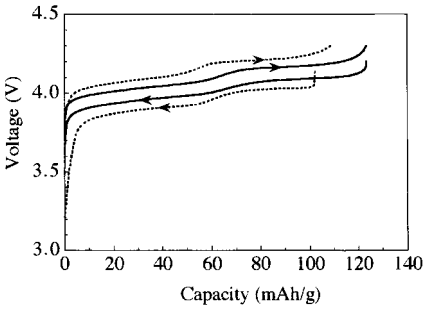

Figure 1. Charge/discharge curve of the spinel $Li_xMn_2O_4$ before (solid line) and after 14 days storage (dashed line) measured at 0.5 mA/cm^2. (→, charge; ←, discharge).

Energy- dispersive X-ray analysis was carried out on an Oxford Link 1000 scanning electron microscope (SEM) with and Isis EDS detector with a beryllium window and 139 eV resolution. The samples were extensively washed with DMC after charging and/or storage and dried by argon flow in the argon glovebox for 2 h. The samples were then mounted in the SEM with carbon tape to facilitate charge dispersion during measurements. All data were taken under the same conditions to avoid scaling issues.

X-ray photoelectron spectroscopy was performed on a HP 5950A ESCA spectrometer with a microchannel plate and resistive anode detector. The system utilized a monochromitized Al Kα X-ray source emitting photons at 1486.6 eV. The samples were attached to the sample rod and grounded by a gold-covered mask. (The opening in the mask is about 7 mm × 4 mm, slightly smaller than the electrode pieces used for the XPS studies.) All binding energies were referenced to the gold $4f^{7/2}$ photoelectron peak at 84.0 eV. All spectra were taken with an electron take off angle of ∼60°.

Results and Discussion

The charge/discharge curves of the $Li_xMn_2O_4$ cathode *before* and *after storage* are shown in Figure 1. *Before storage*, the cathode was charged up to 4.3 V at 0.5 mA/cm^2 and the cathode had a capacity of 124 mA h g^{-1}. One can notice that there are two plateaus in the curve, which correspond to the two-step reversible intercalation/deintercalation of Li^+ ions.[12,14−19] After 2 weeks of

(13) Antonini, A.; Bellitto, C.; Pasquali, M.; Pistoia, G. *J. Electrochem. Soc.* **1998**, *145*, 2726.

(14) Tarascon, J. M.; Guyomard, D. *J. Electrochem. Soc.* **1991**, *138*, 2864.

(15) Rougier, A.; Striebel, K. A.; Wen, S. J.; Cairns, E. J. *J. Electrochem. Soc.* **1998**, *145*, 2975.

(16) Ohzuku, T. ; Kitagawa, M.; Hirai, T. *J. Electrochem. Soc.* **1990**, *137*, 769.

(17) Tarascon, J. M.;, Wang, E.; Shokoohi, F. K.; McKinnon, W. R.; Colson, S. *J. Electrochem. Soc.* **1991**, *138*, 2859.

(18) Amatucci, G. G.; Schmutz, C. N.; Blyr, A.; Sigala, C.; Gozdz, A. S.; Larcher, D.; Tarascon, J. M. *J. Power Sources* **1997**, *69*, 11.

(19) Aurbach, D.; Levi, M. D.; Levi, E.; Teller, H.; Markovsky, B.; Salitra, G.; Heider, U.; Heider, L. *J. Electrochem. Soc.* **1998**, *145*, 3024.

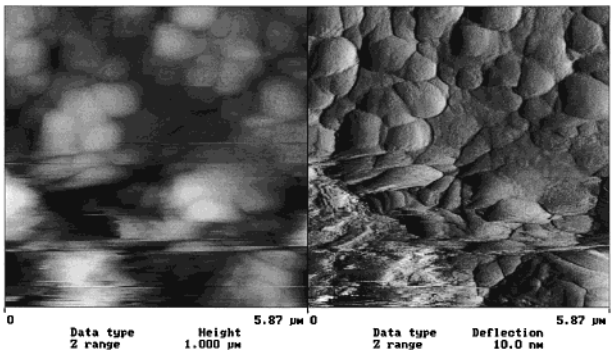

Figure 2. Contact AFM image in height (left) and deflection (right) mode of the initial cathode surface. In the height mode ("constant force" mode), the real topography is shown on a gray scale from 0 to 1 mm.

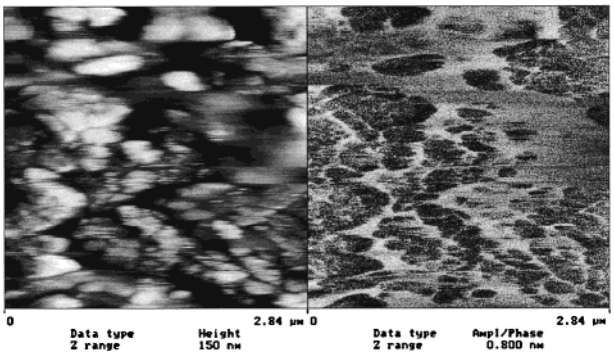

Figure 3. LFM image in height (left) and friction (right) mode of the initial cathode surface. In the force mode, the areas of high friction are bright and the areas of low friction are dark.

storage, the discharge capacity measured at the same current density decreased to 102 mA h g^{-1}, which was an 18% loss of the initial capacity. In addition to the capacity fading, hysteresis between charge and discharge curves became larger *after storage*. Since the hysteresis corresponds to the resistance of the cell, it is clear that *after storage* the resistance of the spinel cathode increased. The increase is well-known and has been summarized by Inoue and Sano.[5]

The contact AFM, LFM, and tapping modes were used to image the topography and phase distribution in the cathode material surface. Typical AFM images of the initial cathode surface are shown in Figures 2 and 3. Figure 2 shows the AFM image of the cathode material in air using contact AFM. At large scan size, loose debris on the surface causes loss of image resolution and produced streaking in the image. In the contact AFM mode, the cantilever constantly contacts the sample throughout the scanning. As a result, debris is often observed, especially at large scan size observation. At a lower scan size, the image becomes more clearly in both height and deflection imaging. The contact AFM mode was not used in any further characterization of the cathode material because of the poor imaging features shown by the composite surface.

Tapping mode AFM minimizes the surface destruction by utilizing a tapping mechanism as the cantilever touches periodically the cathode surface. Therefore, the TM-AFM results in clearer images of the surface topography with more visible details even at large scans, which is more difficult to achieve by contact AFM. Phase imaging can also be performed simultaneously with TM-

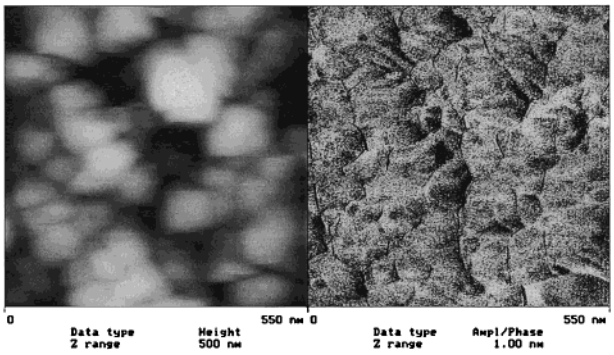

Figure 4. LFM image in height (left) and friction (right) mode of the fully charged cathode material.

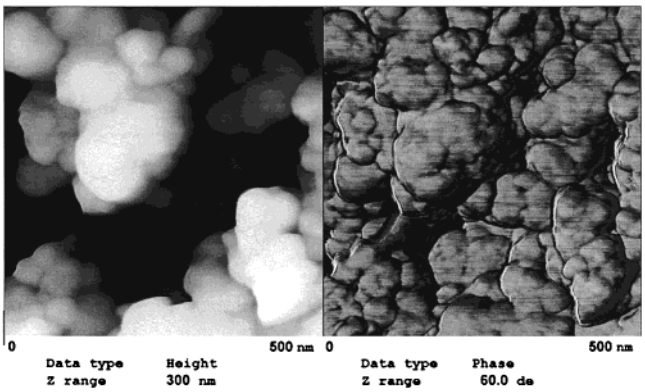

Figure 5. TM-AFM image in height (left) and phase (right) mode of the fully charged cathode material.

AFM to provide additional information about the surface. However, since binder and active material have significant different friction properties, LFM is expected to provide visible contrast between the two phases because the LFM detects the lateral bending of the cantilever, which is often the result of difference in frictional forces between the cantilever and the sample surface. Figure 3 shows the image of the cathode surface in LFM mode on which contrasting binder and active material areas are easily identified. In contact mode, the friction image (right) showed two prominent areas of high friction (bright) and one area of low friction (dark). In the height image (left) there was little topography corresponding to the high friction areas, but there was a raised area corresponding to the low friction area. The binder and carbon black appears to be preferentially concentrated around the $LiMn_2O_4$ particles, which cover about 75% of the cathode surface (this percentage being inferred by the fact that the cathode is comprised of 75 wt % of active material). The $LiMn_2O_4$ crystallites produce large contrast in the phase imaging relative to the remaining binder and carbon black phase. The LFM image of the particles shows that the active material has relatively lower surface friction and adhesion, as the phase imaging is sensitive to these properties. All imaging was subsequently made on the $LiMn_2O_4$ particles, taking care not to image the binder and carbon black.

Typical AFM images of a surface of fully charged cathode materials *before storage* are shown in Figures 4 and 5. Figure 4 presents the LFM image of the charged cathode (121 mA h g^{-1}). Both height (left) and friction (right) images show grainlike morphology. Similar appearance of the cathode surface topography

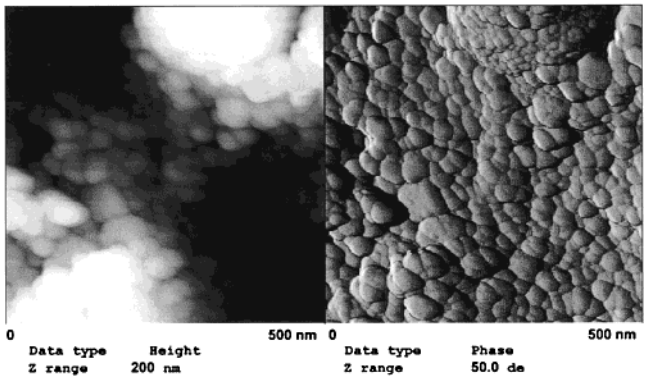

Figure 6. TM-AFM image in height (left) and phase (right) mode of the fully charged cathode *after storage* in the electrolyte of $LiPF_6$/EC + DMC + DEC at 70 °C for 2 weeks.

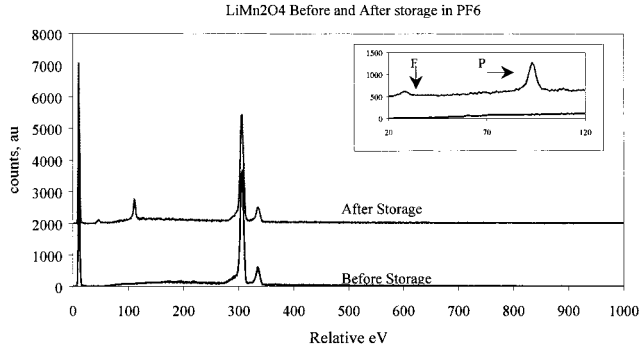

Figure 7. EDAX data for samples both *before* and *after storage* at 70 °C for 5 days: dashed line, *before storage*; solid line, *after storage.*

was observed by TM-AFM. Figure 5 represents the height image (left) and the phase image (right) of the fully charged sample. The phase image reveals the surface morphology with a higher resolution than the height image. Grain boundaries in the phase image have a good correspondence to those in the height image. There exist grains of 100−200 nm in size on the cathode surface *before storage.*

Figure 6 shows TM-AFM images of the surface of the cathode charged to 4.3 V with a capacity of 121 mAh g^{-1}, which was then stored in the electrolyte of $LiPF_6$ /EC + DMC + DEC at 70 °C. Very fine structures of 10−30 nm in size can be detected in the phase image. Beside the grain boundaries of 100−200 nm, which exist on the sample *before storage*, the fine structures of about 10−30 nm appear to be on the larger grains. To our knowledge, these AFM images are the first images made of the spinel cathode before and *after storage.* The fine structures may be formed by decomposition of the supporting salt in the electrolyte on the cathode surface or migration of Mn^{2+} ions to the surface. Compositional changes of the surface could play a role in the increase of resistance of Li ion transport through the cathode interface.

To analyze the composition of the surface, energy-dispersive X-ray analysis (EDAX) was performed. Figure 7 shows EDAX data for samples *before* (lower line) and *after storage* (upper line). Here the Mn peak is clearly visible rising above the characteristic Brongstrum peak. The sample *before storage* shows only the Mn peaks; however, the sample *after storage* shows peaks for phosphorus and fluorine, as seen in the inset. The results indicate that both phosphorus and fluorine

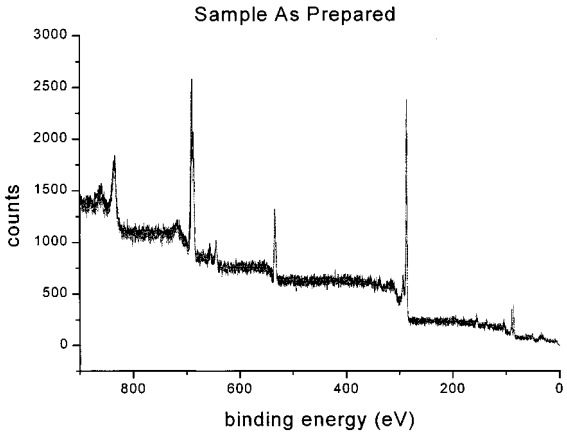

Figure 8. XPS survey scans of sample *before storage.*

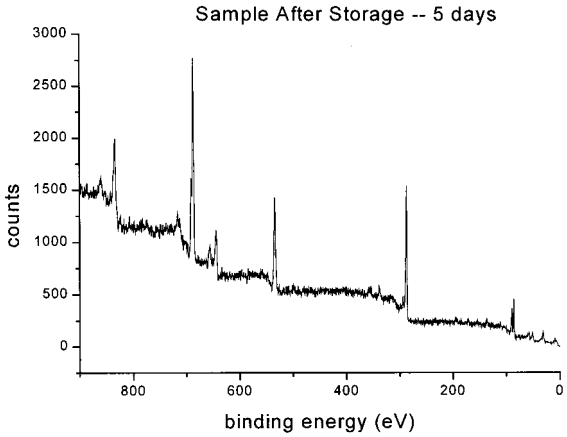

Figure 9. XPS survey scans of sample *after storage.*

have been deposited on the surface from the solution. Therefore, along with Mn^{2+}, other compounds containing phosphorus and fluorine are seen on the surface and may contribute to the fine structures seen by the AFM.

To understand the surface chemistry of the manganese dissolution of the $LiMn_2O_4$, X-ray photoelectron spectroscopy (XPS) was employed. Using XPS, electrons are ejected with kinetic energy equal to the difference between incident photon energy and the electron's binding energy. X-ray photoelectron spectroscopy has the capability of determining compositions of surface constituents by monitoring the shift in the binding energy of core level electrons from the atoms in the surface compounds. Figures 8 and 9 show the survey scans (scans over the whole spectrum) for samples *as prepared* and *after storage* for 5 days, respectively. Here the major features presented are, from left to right, fluorine KLL Auger electron peaks (~860 and 833 eV when using $h\nu$ = 1486.6 eV) and photoelectron peaks from electronic states F 1s (~689 and 686 eV), Mn 2p (~639 eV), O 1s (~535 eV), C 1s (287 eV), and the Au $4f^{5/2}$ and $4f^{7/2}$ (~87.7 and 84.0 eV). When the scans are compared in the areas of the fluorine and manganese photoelectron peaks, significant differences can be observed. Figures 10−12 show the fluorine 1s photoelectron spectra for the *as prepared*, *charged before storage*, and *after storage* samples. The peaks were fitted in the following manner. The photoelectron peaks were fit using Voigt functions: a convolution of Gaussian functions to account for instrument uncertainties; Lorentzian functions to approximate the natural energy line

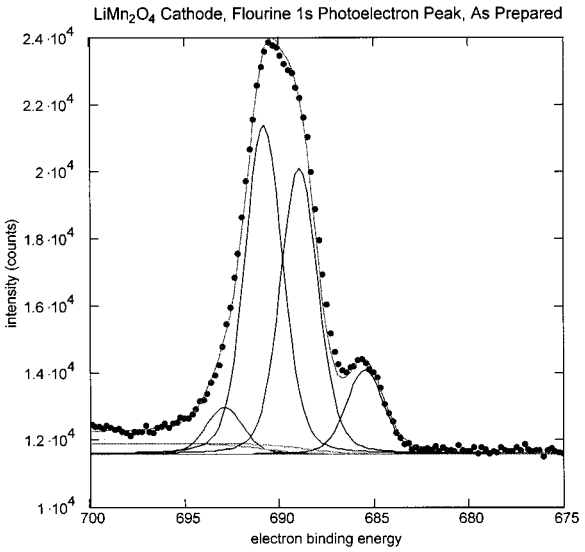

Figure 10. XPS data (points) and approximate fits (lines) for the F 1s region, *as prepared*.

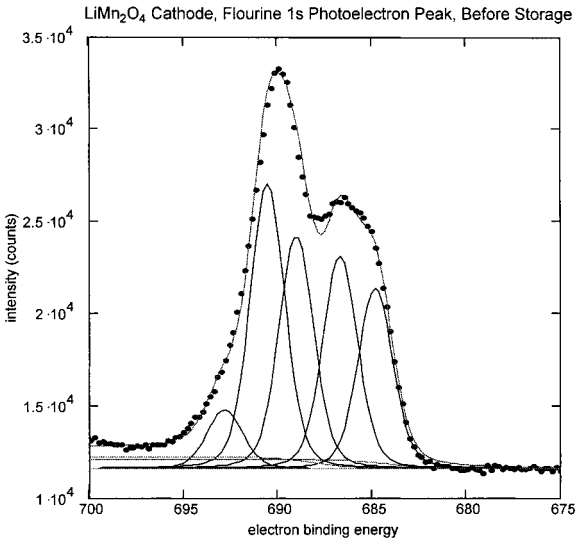

Figure 11. XPS data (points) and approximate fits (lines) for the F1s region, *before storage.*

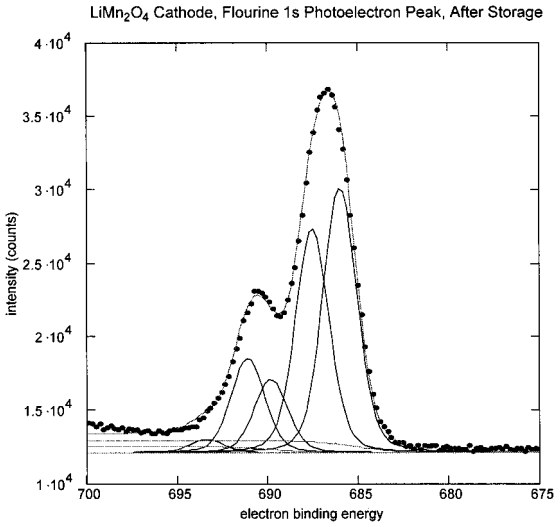

Figure 12. XPS data (points) and approximate fits (lines) for the F1s region, *after storage.*

widths. The background was fit using sigmoidal functions centered on major features. The full-width-half-maxima of all Voigt functions are fixed and were found from measurements on the instrument used by spectra from a similar sample with one fluorine feature. The value of approximately 1.95 eV agrees with a previous study using a similar instrument.[20] Each feature is in the spectra is due to fluorine atoms in a particular chemical state. Figure 10 shows a doublet of the fluorine 1s peak for the *as prepared* sample (a spacing of approximately 1.8 eV). The broad left peak in the fluorine 1s is due to tribological stresses put on the Teflon during fabrication.[21] The smaller peak on the right can be attributed to a small amount of MnF_2 (684.6 eV) formation.[22] An alternative assignment for the smaller peak is LiF (also at 684.4 eV).[22] However, after the cathode was charged, the lithium in the cathode should be completely depleted, especially the surface region. Figure 11 shows a growth of the peak after charging which is inconsistent with the assignment of this peak to LiF because of the depletion of Li from the surface region. Therefore, we believe this peak is due to MnF_2.

The deconvoluted peaks in Figure 10 from left to right correspond to a satellite Teflon (resonance effects of CF_3 and CF_2 at ~694 eV), CF_3 (~691 eV), CF_2 (~689 eV), and MnF_2 (~684.4 eV). In the sample that was charged, but not stored (Figure 11), the MnF_2 peak grows larger, along with a new feature about 1.3 eV higher that can be attributed to PF_5 (and/or PF_6) at 687 eV. This new feature was completely absent in samples used for referencing the Voigt functions (these reference samples were stored in a $LiClO_4$ electrolyte rather than the $LiPF_6$ electrolyte). Figure 11 indicates that the MnF_2 peak, which has a binding energy of ~685 eV, is beginning to grow even *before storage*. In the sample *after storage*, the right-hand peak becomes dominant over both Teflon peaks (Figure 12). The formation of MnF_2 on the surface has increased dramatically enough to dwarf the formerly large CF_3 and CF_2 peaks. Deconvolution of the peaks in Figure 12 shows a dramatic increase in MnF_2 and PF_5 (and/or PF_6) concentrations at the surface. The formation of MnF_2 on the surface of the cathode is a byproduct of charging, but more importantly it is also a product of storage at elevated temperatures.

Additional information can be obtained from the manganese peak. From the survey scan (see Figure 9) and the major manganese 2p peaks (~639 eV), there seems to be little difference between the three scans. However, looking at the 3s/3p (~48 and 82 eV) region for manganese in the scan, there is an important difference. Nelson et al.[23] performed studies on various manganese compounds in this region. Specifically, one study showed that the state of manganese could be determined by the change in the doublet splitting of the 3s peaks. Figures 13−15 show the manganese 3s/3p peaks for samples *as prepared*, *charged before storage*,

(20) Beard, B. C.; Brizzolara, R. A. *Surf. Sci. Spectra* **1993**, *2*, 8.
(21) Li, F.; Yan, F.; Yu, L.; Liu, W. *Wear* **2000**, *237*, 33.
(22) Wagner C. D.; Muilenberg, G. E. *Handbook of X-ray Photoelectron Spectroscopy*; Perkin-Elmer Corp.: Eden Prairie, MN, 1979; p 169.

(23) Nelson, A. J.; Reynolds, J. G.; Roos, J. W. *J. Vac. Sci. Technol., A* **2000**, *18*, 1072.

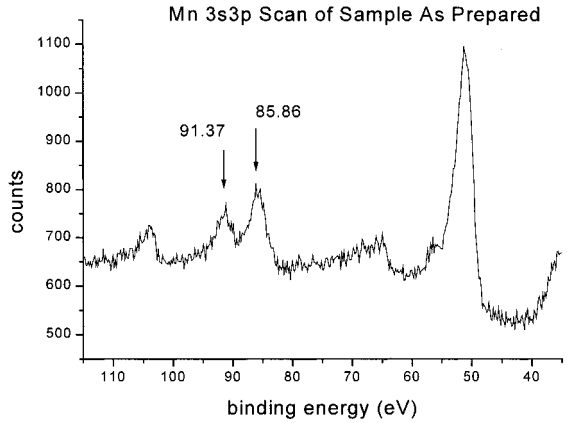

Figure 13. XPS scan of manganese 3s 3p peaks of sample *as prepared*.

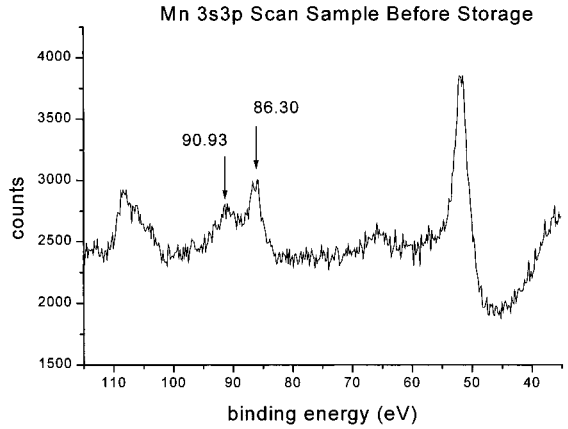

Figure 14. XPS scan of manganese 3s 3p peaks of sample charged *before storage*.

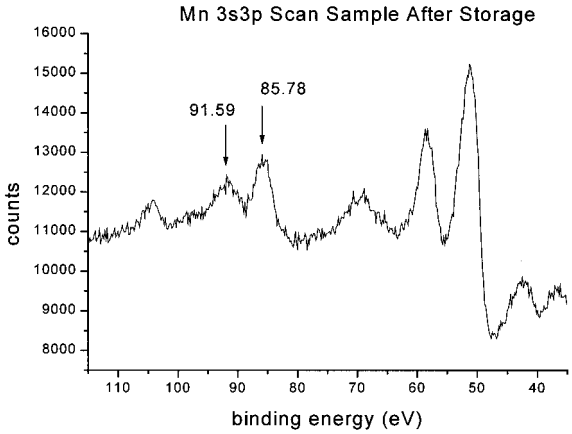

Figure 15. XPS scan of manganese 3s 3p peaks of sample *after storage*.

and *after storage*, respectively. The relative difference in energy for these the 3s doublet splitting is 5.51, 4.63, and 5.81 eV, respectively. Nelson et al.[23] found that for MnO and Mn_3O_4 the difference was 5.6 eV, for Mn_2O_3 it was 5.4 eV, and for MnO_2 it was 4.5 eV. This indicates that the *as prepared manganese state* is similar to Mn_2O_3, which has manganese in the Mn^{3+} state. In the *as prepared state* ($LiMn_2O_4$), the manganese should be an average of $Mn^{3+.5}$ (being a combination of both Mn^{3+} and Mn^{4+}). As expected, the sample *before storage*, which is completely delithiated, has a 3s doublet split corresponding to the MnO_2 state.[22] The sample *after storage* has a doublet split of 5.81 eV, which indicates that the sample is MnO. Thus, during storage the surface of the cathode material changes state from MnO_2 to predominately MnO. The results are consistent with a possible degradation mechanism wherein the $LiPF_6$ salt dissociates reversibly to LiF and PF_5. The PF_5 can in turn react with the manganese oxides on the surface to form manganese difluoride on the cathode and soluble products in the electrolyte.[24] The soluble products in the electrolyte could be POF_3 and PO_2F_2.[24] Free energy calculations show negative values for the formation of the surface and soluble products.[24] The proposed reaction mechanisms by Tasaki[24] are consistent with the results reported here. However, it is possible that the organics in the electrolyte also participate in the cathode surface modification processes, and our future work will focus on measuring changes both in the electrolyte and on the cathode surface during elevated temperature storage.

Conclusion

The surface of the spinel $Li_xMn_2O_4$ before and *after storage* at elevated temperature was investigated and correlated with the change in electrochemical properties. One of the reasons for the capacity fading *after storage* at elevated temperatures is the increase of the electrode resistance. The formation of films on the cathode causes a resistance increase and, consequently, capacity fading. The surface of the cathode material was observed by AFM, and fine grains of nearly round shapes and 10−30 nm in size were detected *after storage*. This structure appears to be due to the presence of MnF_2 being deposited on the surface, as seen by XPS. Furthermore, the state of manganese changes from MnO_2 to MnO during storage at the elevated temperature, which may also create Mn^{2+} deposition on the surface. The information obtained in this study is useful in determining a mechanism for cathode surface deterioration and surface film formation.

Acknowledgment. The authors thank Mr. S. Kinoshita of MCC for discussions and assistance in the experiments. Also, we thank the Fadley Group at UC Davis. This work was supported in part by Mitsubishi Chemical Corp. (MCC).

CM010335V

(24) Tasaki, K. Private communication, MC Research and Innovation Center, Inc., Mountain View, CA 2001.